(23-A-9); by Grants-in-Aid for Scientific Research by the Japan Society for the Promotion of Science; by Grants-in-Aid for Scientific Research on Innovative Areas by the Ministry of Education, Culture, Sports, Science and Technology of Japan; and by a Grant-in-Aid from the Ministry of Health, Labour and Welfare of Japan for the 3rd Term Comprehensive 10-year Strategy for Cancer Control. This work was also supported in part by The Mochida Memorial Foundation for Medical and Pharmaceutical Research and The Sagawa Foundation for Promotion of Cancer Research.

Disclosure Statement

The authors have no conflict of interest.

References

1 Lauren P. The two histological main types of gastric carcinoma: diffuse and so-called intestinal-type carcinoma. An attempt at a histo-clinical classification. *Acta Pathol Microbiol Scand* 1965; **64**: 31–49.
2 Jinawath N, Furukawa Y, Hasegawa S *et al.* Comparison of gene-expression profiles between diffuse- and intestinal-type gastric cancers using a genome-wide cDNA microarray. *Oncogene* 2004; **23**: 6830–44.
3 Ming SC. Cellular and molecular pathology of gastric carcinoma and precursor lesions: a critical review. *Gastric Cancer* 1998; **1**: 31–50.
4 Sipponen P. Gastric cancer: pathogenesis, risks, and prevention. *J Gastroenterol* 2002; **37** (Suppl. 13): 39–44.
5 Yashiro M, Hirakawa K. Cancer-stromal interactions in scirrhous gastric carcinoma. *Cancer Microenviron* 2010; **3**: 127–35.
6 Ikeguchi M, Miyake T, Matsunaga T *et al.* Recent results of therapy for scirrhous gastric cancer. *Surg Today* 2009; **39**: 290–4.
7 Otsuji E, Kuriu Y, Okamoto K *et al.* Outcome of surgical treatment for patients with scirrhous carcinoma of the stomach. *Am J Surg* 2004; **188**: 327–32.
8 Hattori Y, Itoh H, Uchino S *et al.* Immunohistochemical detection of K-sam protein in stomach cancer. *Clin Cancer Res* 1996; **2**: 1373–81.
9 Hattori Y, Odagiri H, Nakatani H *et al.* K-sam, an amplified gene in stomach cancer, is a member of the heparin-binding growth factor receptor genes. *Proc Natl Acad Sci USA* 1990; **87**: 5983–7.
10 Kuniyasu H, Yasui W, Kitadai Y, Yokozaki H, Ito H, Tahara E. Frequent amplification of the c-met gene in scirrhous type stomach cancer. *Biochem Biophys Res Commun* 1992; **189**: 227–32.
11 Trusolino L, Bertotti A, Comoglio PM. MET signalling: principles and functions in development, organ regeneration and cancer. *Nat Rev Mol Cell Biol* 2010; **11**: 834–48.
12 Comoglio PM, Giordano S, Trusolino L. Drug development of MET inhibitors: targeting oncogene addiction and expedience. *Nat Rev Drug Discov* 2008; **7**: 504–16.
13 Cecchi F, Rabe DC, Bottaro DP. Targeting the HGF/Met signalling pathway in cancer. *Eur J Cancer* 2010; **46**: 1260–70.
14 Liu X, Newton RC, Scherle PA. Development of c-MET pathway inhibitors. *Expert Opin Investig Drugs* 2011; **20**: 1225–41.
15 Lee J, Seo JW, Jun HJ *et al.* Impact of MET amplification on gastric cancer: possible roles as a novel prognostic marker and a potential therapeutic target. *Oncol Rep* 2011; **25**: 1517–24.
16 Toiyama Y, Yasuda H, Saigusa S *et al.* Co-expression of hepatocyte growth factor and c-Met predicts peritoneal dissemination established by autocrine hepatocyte growth factor/c-Met signaling in gastric cancer. *Int J Cancer* 2012; **130**: 2912–21.
17 Turner N, Grose R. Fibroblast growth factor signalling: from development to cancer. *Nat Rev Cancer* 2010; **10**: 116–29.
18 Dieci MV, Arnedos M, Andre F, Soria JC. Fibroblast growth factor receptor inhibitors as a cancer treatment: from a biologic rationale to medical perspectives. *Cancer Discov* 2013; **3**: 264–79.
19 Kawakami H, Okamoto I, Arao T *et al.* MET amplification as a potential therapeutic target in gastric cancer. *Oncotarget* 2013; **4**: 9–17.
20 McDermott U, Sharma SV, Dowell L *et al.* Identification of genotype-correlated sensitivity to selective kinase inhibitors by using high-throughput tumor cell line profiling. *Proc Natl Acad Sci USA* 2007; **104**: 19936–41.
21 Nakagawa T, Tohyama O, Yamaguchi A *et al.* E7050: a dual c-Met and VEGFR-2 tyrosine kinase inhibitor promotes tumor regression and prolongs survival in mouse xenograft models. *Cancer Sci* 2010; **101**: 210–5.
22 Okamoto W, Okamoto I, Arao T *et al.* Antitumor action of the MET tyrosine kinase inhibitor crizotinib (PF-02341066) in gastric cancer positive for MET amplification. *Mol Cancer Ther* 2012; **11**: 1557–64.
23 Okamoto W, Okamoto I, Yoshida T *et al.* Identification of c-Src as a potential therapeutic target for gastric cancer and of MET activation as a cause of resistance to c-Src inhibition. *Mol Cancer Ther* 2010; **9**: 1188–97.
24 Smolen GA, Sordella R, Muir B *et al.* Amplification of MET may identify a subset of cancers with extreme sensitivity to the selective tyrosine kinase inhibitor PHA-665752. *Proc Natl Acad Sci USA* 2006; **103**: 2316–21.
25 Kunii K, Davis L, Gorenstein J *et al.* FGFR2-amplified gastric cancer cell lines require FGFR2 and Erbb3 signaling for growth and survival. *Cancer Res* 2008; **68**: 2340–8.
26 Nakamura K, Yashiro M, Matsuoka T *et al.* A novel molecular targeting compound as K-samII/FGF-R2 phosphorylation inhibitor, Ki23057, for Scirrhous gastric cancer. *Gastroenterology* 2006; **131**: 1530–41.
27 Yashiro M, Shinto O, Nakamura K *et al.* Synergistic antitumor effects of FGFR2 inhibitor with 5-fluorouracil on scirrhous gastric carcinoma. *Int J Cancer* 2010; **126**: 1004–16.
28 Hara T, Ooi A, Kobayashi M, Mai M, Yanagihara K, Nakanishi I. Amplification of c-myc, K-sam, and c-met in gastric cancers: detection by fluorescence *in situ* hybridization. *Lab Invest* 1998; **78**: 1143–53.
29 Nessling M, Solinas-Toldo S, Wilgenbus KK, Borchard F, Lichter P. Mapping of chromosomal imbalances in gastric adenocarcinoma revealed amplified protooncogenes MYCN, MET, WNT2, and ERBB2. *Genes Chromosom Cancer* 1998; **23**: 307–16.
30 Sakakura C, Mori T, Sakabe T *et al.* Gains, losses, and amplifications of genomic materials in primary gastric cancers analyzed by comparative genomic hybridization. *Genes Chromosom Cancer* 1999; **24**: 299–305.
31 Yanagihara K, Seyama T, Tsumuraya M, Kamada N, Yokoro K. Establishment and characterization of human signet ring cell gastric carcinoma cell lines with amplification of the c-myc oncogene. *Cancer Res* 1991; **51**: 381–6.
32 Yanagihara K, Takigahira M, Takeshita F *et al.* A photon counting technique for quantitatively evaluating progression of peritoneal tumor dissemination. *Cancer Res* 2006; **66**: 7532–9.
33 Yanagihara K, Takigahira M, Tanaka H *et al.* Development and biological analysis of peritoneal metastasis mouse models for human scirrhous stomach cancer. *Cancer Sci* 2005; **96**: 323–32.
34 Yanagihara K, Tanaka H, Takigahira M *et al.* Establishment of two cell lines from human gastric scirrhous carcinoma that possess the potential to metastasize spontaneously in nude mice. *Cancer Sci* 2004; **95**: 575–82.
35 Yamaguchi H, Yoshida S, Muroi E *et al.* Phosphoinositide 3-kinase signaling pathway mediated by p110alpha regulates invadopodia formation. *J Cell Biol* 2011; **193**: 1275–88.
36 Ueda T, Sasaki H, Kuwahara Y *et al.* Deletion of the carboxyl-terminal exons of K-sam/FGFR2 by short homology-mediated recombination, generating preferential expression of specific messenger RNAs. *Cancer Res* 1999; **59**: 6080–6.
37 Catenacci DV, Henderson L, Xiao SY *et al.* Durable complete response of metastatic gastric cancer with anti-Met therapy followed by resistance at recurrence. *Cancer Discov* 2011; **1**: 573–9.
38 Humar B, Fukuzawa R, Blair V *et al.* Destabilized adhesion in the gastric proliferative zone and c-Src kinase activation mark the development of early diffuse gastric cancer. *Cancer Res* 2007; **67**: 2480–9.
39 Hagiwara A, Takahashi T, Sawai K *et al.* Milky spots as the implantation site for malignant cells in peritoneal dissemination in mice. *Cancer Res* 1993; **53**: 687–92.
40 Guarino M. Src signaling in cancer invasion. *J Cell Physiol* 2010; **223**: 14–26.

Supporting Information

Additional supporting information may be found in the online version of this article:

Fig. S1. Purification and identification of tyrosine-phosphorylated proteins in 58As9 cells.

Fig. S2. Effects of Met inhibitors on cell growth and signaling in 44As3 and 58As9 cells.

Fig. S3. Effect of simultaneous addition of Met and Src inhibitors on proliferation of 58As9 cells.

Fig. S4. Effects of Met, fibroblast growth factor receptor (FGFR), and Src inhibitors on intracellular signaling pathways in diffuse-type gastric carcinoma (DGC) cell lines.

Fig. S5. Effect of saracatinib on proliferation of intestinal-type gastric carcinoma cell lines.

Table S1. List of cell lines used in this study.

OPEN ACCESS Freely available online

PLOS ONE

Stromal Fibroblasts Mediate Extracellular Matrix Remodeling and Invasion of Scirrhous Gastric Carcinoma Cells

Hideki Yamaguchi[1], Nachi Yoshida[1], Miho Takanashi[1,2], Yuumi Ito[1,2], Kiyoko Fukami[2], Kazuyoshi Yanagihara[3], Masakazu Yashiro[4], Ryuichi Sakai[1]*

1 Division of Metastasis and Invasion Signaling, National Cancer Center Research Institute, Chuo-ku, Tokyo, Japan, **2** Laboratory of Genome and Biosignal, Tokyo University of Pharmacy and Life Sciences, Hachioji-shi, Tokyo, Japan, **3** Research Center for Innovative Oncology, National Cancer Center Hospital East, Kashiwa-City, Chiba, Japan, **4** Department of Surgical Oncology, Osaka City University Graduate School of Medicine, Abeno-ku, Osaka, Japan

Abstract

Scirrhous gastric carcinoma (SGC) has the worst prognosis of all gastric cancers, owing to its rapid expansion by invasion and frequent peritoneal dissemination. Due to the increased proliferation of stromal fibroblasts (SFs) that occurs within SGC lesions and the peritoneal metastatic sites, SFs have been proposed to support the progression of this disease. However, the biological and molecular basis and the pathological role of the intercellular interaction between SGC cells and SFs remain largely unknown. In this study, we investigated the role of SFs in the invasion of the extracellular matrix (ECM) by SGC cells. When SGC cells were cocultured with SFs derived from SGC tissue on three-dimensional (3D) Matrigel, they were attracted together to form large cellular aggregates that invaded within the Matrigel. Time-lapse imaging revealed that this process was associated with extensive contraction and remodeling of the ECM. Immunofluorescence and biochemical analysis showed that SGC cells stimulate phosphorylation of myosin light chain and actomyosin-mediated mechanical remodeling of the ECM by SFs. By utilizing this assay system for inhibitor library screening, we have identified several inhibitors that potently suppress the cooperation between SGC cells and SFs to form the invasive structures. Among them, a Src inhibitor dasatinib impaired the interaction between SGC cells and SFs both in vitro and in vivo and effectively blocked peritoneal dissemination of SGC cells. These results indicate that SFs mediate mechanical remodeling of the ECM by SGC cells, thereby promoting invasion and peritoneal dissemination of SGC.

Citation: Yamaguchi H, Yoshida N, Takanashi M, Ito Y, Fukami K, et al. (2014) Stromal Fibroblasts Mediate Extracellular Matrix Remodeling and Invasion of Scirrhous Gastric Carcinoma Cells. PLoS ONE 9(1): e85485. doi:10.1371/journal.pone.0085485

Editor: Alissa M. Weaver, Vanderbilt University Medical Center, United States of America

Received July 16, 2013; **Accepted** November 27, 2013; **Published** January 10, 2014

Funding: This work was supported by Grants-in-Aid for Scientific Research by the Japan Society for the Promotion of Science; by Grants-in-Aid for Scientific Research on Innovative Areas by the Ministry of Education, Culture, Sports, Science and Technology of Japan; and by a Grant-in-Aid from the Ministry of Health, Labour and Welfare of Japan for the 3rd term Comprehensive 10-year Strategy for Cancer Control. This work was supported in part by the National Cancer Center Research and Development Fund (23-A-9), and also by Grant-in-Aid from the Tokyo Biochemical Research Foundation. The funders had no role in study design, data collection and analysis, decision to publish, or preparation of the manuscript.

Competing Interests: The authors have declared that no competing interests exist.

* E-mail: rsakai@ncc.go.jp

Introduction

Recent studies have established the importance of the tumor stroma in cancer progression [1,2]. Tumor stroma consists of many types of non-cancerous cells and non-cellular components including the extracellular matrix (ECM). Stromal fibroblasts (SFs) are major cellular constituents of tumor stroma and often called cancer-associated fibroblasts (CAFs) [3]. They have been implicated in the malignant behavior of cancers, such as cell proliferation, ECM remodeling, and angiogenesis [4]. Moreover, they often display the phenotypes of myofibroblasts, characterized by the expression of α-smooth muscle actin (αSMA) and strong contractility [5]. These characteristics contribute not only to fibrosis in tumor tissue but also to the remodeling and stiffening of the stromal ECM that are favorable for invasion and metastasis of carcinoma cells [6,7].

Scirrhous gastric carcinoma (SGC), also known as diffusely infiltrative carcinoma, has a very poor prognosis due to rapid infiltrative invasion and a high incidence of peritoneal dissemination [8,9]. SGC is associated with extensive stromal fibrosis, resulting in the thickening and hardening of the gastric wall and shrinkage of the stomach. As there is elevated proliferation of SFs in SGC lesions, they have been proposed to support the progression of this disease [10]. In fact, a positive correlation between the presence of SFs and the metastatic potential of gastric cancers has been found [11]. SGC cells induce fibrosis of the peritoneum in peritoneal dissemination, indicating that SFs also play a role here [12]. Recent studies have demonstrated that SFs stimulate migration and invasion of SGC cells [13,14] and SGC cells reciprocally promote proliferation of gastric fibroblasts [14,15]. However, the biological and molecular basis and the pathological function of the intercellular interaction between SGC cells and SFs remain largely unknown. In this study, we established the system to visualize and quantify the crosstalk between SFs and SGC cells for achieving the invasive properties and investigated the role of SFs in the invasion and remodeling of the ECM by SGC cells.

Materials and Methods

Cell culture

Human gastric cancer cell lines 58As9, HSC-59, HSC-44PE, and 44As3 were described previously [16,17], and MKN1, MKN7, and MKN74 were obtained from the Health Science Research Resources Bank. 44As3 cells stably expressing tdTomato were generated by retroviral transduction. These cells were maintained in RPMI 1640 medium (Invitrogen) supplemented with 10% FBS and antibiotics at 37°C in a humidified atmosphere containing 5% CO_2. The orthotopic fibroblast cell lines, CaF37 and CaF38 were established from the tumoral gastric wall of SGC patients who had undergone gastrectomy. The primary gastric tumor was excised under aseptic conditions and minced with forceps and scissors. The tumor pieces were cultivated in DMEM (Nikken) with 10% FBS. After approximately 2 weeks, fibroblasts were collected and transferred to another culture dish. Serial passages were carried out every 4–7 days. The fibroblasts used were 4–10th passage of culture. This study was approved by the Osaka City University ethics committee and written informed consent was obtained from the patients prior to the study.

Reagents

Fluorescent phalloidin and secondary antibodies, CellTracker, and FluoSpheres polystyrene microspheres (1.0 μm, red fluorescent, 580/605) were purchased from Invitrogen. Matrigel was purchased from BD Biosciences. Inhibitors used were; GM6001, blebbistatin, and PP2 (Merck), dasatinib (Selleck Chemicals), and H1152 and imatinib (Cayman Chemical).

Immunoblotting

Immunoblotting was performed as described previously [18]. Protein concentration was determined with the BCA protein assay kit (Pierce). Following antibodies were used: αSMA, α-tubulin, and ß-actin (Sigma-Aldrich) at 1:5000 dilution; myosin light chain 2 (MLC2), phospho-MLC2 (Ser19), phospho-MLC2 (Thr18/Ser19), Src, phospho-Src (Tyr416), and vimentin (Cell Signaling Technology) at 1:1000 dilution.

3D Matrigel invasion assay

Matrigel was placed in 24-well plates (250 μl/well) or on cover slips (12-mm, circular; 40 μl/cover slip) and solidified at 37°C for 1 h. SGC cells (2×10^4) and SFs (5×10^4) were plated onto 3D Matrigel and cultured for 2 days. To visualize ECM remodeling, Matrigel was mixed with FluoSpheres polystyrene microspheres at 2×10^3 beads/ml. To calculate the number of invasive foci, Matrigel-containing plates were scanned and analyzed with the particle counting function of the ImageJ 1.41o software. Cell aggregates larger than 0.05 mm^2 in area were counted in this analysis. In each experiment, the values of control cells were set to 1 and the relative values of other cells were then calculated accordingly. To calculate the number and areas of cell clusters, cells in six randomly selected fields were imaged with a 10× objective and analyzed with the ImageJ 1.41o software. Invasion depth of invasive foci was determined by confocal microscopy.

Gelatin remodeling assay

Fluorescent gelatin-coated cover slips were prepared as described previously [19]. Cells were cultured on the gelatin-coated cover slips for 16 h. To quantitate the gelatin remodeling activity, areas where the fluorescent gelatin was detached were calculated in microscopic images using the ImageJ 1.41o software. Ten randomly selected fields were imaged with a 20× objective and analyzed for each experiment. The values of control cells were set to 100, and the relative values of other cells were then calculated accordingly.

Immunofluorescence and time-lapse microscopy

Immunofluorescence was performed as described previously [19]. Phospho-MLC2 (Ser 19) antibody was used at 1:50 dilution. FSP1/S100A4 antibody (Millipore) was used at 1:200 dilution. Samples were observed with an Olympus IX81-ZDC-DSU microscope equipped with a cooled CCD camera (ORCA-ER, Hamamatsu), and the imaging system was driven by MetaMorph software (Universal Imaging). For Time-lapse microscopy, 44As3 cells (1×10^4) and CaF37 cells (2.5×10^4) were plated onto 3D Matrigel (120 μl/well) solidified in a multi-well glass bottom dish (Matsunami). To quantitate ECM remodeling, digital images were converted using ImageJ 1.41o and the movement of microbeads was analyzed. Total distance moved during the time-lapse imaging was calculated for each microbead and normalized by the average value in 44As3 cells. The total and net migration distances of cells before the formation of invasive foci were determined from the time-lapse movies with the manual tracking function of the ImageJ 1.41o software.

Cell growth assay

Cells were plated onto 96-well plates at 4×10^3/well and cultured for 2 days in the presence of inhibitors. Cell growth was determined using a Premix WST-1 Cell Proliferation Assay System (Takara) according to manufacturer instructions. Absorbance at 450 nm was measured with an iMark microplate reader (Bio-Rad Laboratories). The average values of cells treated with DMSO were set to 1, and the relative values of other cells were then calculated accordingly.

Cytotoxicity assay

Cells were plated onto 96-well plates at 1×10^4/well and cultured for 1 day in growth medium. Medium was replaced with RPMI1640 containing 1% FBS and cultured for 2 days in the presence of inhibitors. Cytotoxicity was then determined using a LDH Cytotoxicity Detection Kit (Takara) according to manufacturer instructions. Absorbance at 490 nm was measured with an iMark microplate reader (Bio-Rad Laboratories). The average values of cells treated with 1% Triton X-100 were set to 1, and the relative values of other cells were then calculated accordingly.

Inhibitor screening

SCADS inhibitor kit was kindly provided by Screening Committee of Anticancer Drugs, Japan. Matrigel was placed in μ-Slide Angiogenesis (ibidi, 10 μl/well) and solidified at 37°C for 1 h. SGC cells (2×10^3) and SFs (5×10^3) labeled with CellTracker were cultured in each well in the presence of the inhibitor library (10 μM) for 2 days. The μ-Slide chambers were scanned and the number of invasive foci was calculated. The cells were also observed by fluorescent microscopy and the formation of invasive foci was evaluated.

Peritoneal dissemination assay

44As3 (5×10^5) cells were inoculated intraperitoneally into 6-week-old BALB/c nude mice purchased from CLEA Japan (Tokyo, Japan). Dasatinib (50 mg/kg) were administrated by intraperitoneal injection, thrice a week, starting at a day after the inoculation. At 10 days after inoculation, the mice were sacrificed and dissected. Peritoneal dissemination, liver metastasis, and ascites formation were examined. The number of mesentery nodules larger than 1 mm in diameter was also determined. The

mesentery nodules were paraffin-embedded, sectioned, and subjected to hematoxylin and eosin staining and immunohistochemistry for histological analysis. For immunofluorescence, mesenteries bearing tdTomato-labeled 44As3 tumor nodules were isolated at 3 days after inoculation. These experiments were approved by the Committee for Ethics of Animal Experimentation and conducted in accordance with the guidelines for Animal Experiments in the National Cancer Center.

Statistical analysis

Data are representative of at least 3 independent experiments. Statistical analysis was performed using Student's *t*-tests, ANOVA with Tukey's test, or Mann-Whitney test.

Results

SGC cells and SFs form invasive foci on 3D Matrigel

44As3 SGC cells and CaF37 fibroblasts derived from SGC tissue were labeled with different fluorescent dyes and cultured individually or together, on either Matrigel-coated culture dishes (2D) or the more physiological 3D Matrigel matrices. 44As3 cells cultured on 2D Matrigel were adherent to the substrate but showed less cell-cell adhesions (Fig. 1A). CaF37 cells spread on the substrate and had a spindle morphology. Their morphologies did not significantly change when these cells were cultured together on the 2D substrate. 44As3 cells cultured on 3D Matrigel exhibited rounded morphology and formed flat cell clusters, without showing significant invasion into the matrix (Fig. 1B). CaF37 fibroblasts also showed rounded morphology with small membrane protrusions on 3D Matrigel and formed invasive small cell aggregates reaching as deep as approximately 30 μm in average (Fig. 1B and Fig. S1A). When 44As3 and CaF37 cells were cocultured on 3D Matrigel, they formed large aggregates that consist of a sphere-shaped core and surrounding cells (Fig. 1B). These cellular aggregates invaded as deep as approximately 70 μm in average into the Matrigel, indicating greater invasiveness with this coculture compared to the CaF37 cells alone (Fig. S1A). CaF37 fibroblasts localized almost exclusively in the invading core structures and most of the surrounding and co-invading cells were 44As3 cells (Fig. 1B). We hereafter refer to these invasive cellular aggregates formed by SGC cells and SFs as invasive foci. Addition of conditioned medium from 44As3 cells to CaF37 cells, or vice versa, did not affect the behavior of CaF37 or 44As3 cells (Fig. S1B), suggesting that a direct association between the 2 cell types is important for the formation of invasive foci.

Coculture of 44As3 and CaF37 cells markedly increased the number of invasive foci on 3D Matrigel compared to individual cultures (Fig. S1C and D). Similar results were obtained from 44As3 cells cocultured with CaF38 fibroblasts, also isolated from SGC tissue (Fig. S2A and B). Coculture of non-SGC cell lines MKN7 (well-differentiated tubular adenocarcinoma), MKN1 (adenosquamous carcinoma), and MKN74 (moderately differentiated tubular adenocarcinoma) with CaF37 resulted in formation of sparse and small cell aggregates, with little invasive potential (Fig. 1C and D). In contrast, SGC cell lines 58As9, HSC-44PE, and HSC-59 formed large invasive foci with CaF37 cells, which were comparable to those formed by 44As3 and CaF37 cells (Fig. 1C and D). These observations indicate that the formation of invasive foci is distinctive for SGC cells.

Formation of invasive foci is associated with extensive remodeling of ECM

Time-lapse imaging showed that 44As3 and CaF37 cells exhibited strong migratory phenotypes on 3D Matrigel and gradually gathered to form small clusters, which then coalesced to form large cellular aggregates as time elapsed (Fig. 2A and Video S1). In this example, CaF37 cells within the cell clusters formed long cell protrusions that interacted with each other to attract 2 cell clusters together, resulting in larger cell clusters containing attached 44As3 cells throughout this process. In some cases, 44As3 cells lined up and formed chain-like structures, often on the protrusions of CaF37 cells, which interconnected with small clusters of CaF37 cells. These observations suggest that SGC cells and SFs have strong physical interactions with each other, which contribute to the formation of invasive foci.

Remodeling of ECM was also visualized by tracking the movement of fluorescent microbeads (1.0 μm in diameter) that were seeded in the Matrigel (Fig. 2B and C). When 44As3 cells were cultured alone, the microbeads showed only a slight movement (Video S2). CaF37 cells induced more obvious movement of the microbeads toward each cell cluster (Video S3). When these cells were cultured together, the microbeads showed extensive and long movement along the migratory paths of the cell clusters, finally accumulating around the invasive foci (Video S4). These results indicate that the coculture generated a contraction force during the formation of invasive foci, which resulted in mechanical remodeling and deformation of the ECM.

To characterize further the ECM remodeling activity of SFs, we cultured 44As3 and CaF37 cells on fluorescent gelatin-coated cover slips (Fig. 2D and E). 44As3 cells did not affect the integrity of the gelatin matrix. CaF37 cells induced remodeling of the gelatin matrix as shown by the appearance of black regions. This activity was markedly enhanced when they were cocultured with 44As3 cells. Similar results were obtained when CaF38 cells were used (Fig. S2C and D). This gelatin remodeling activity was not blocked by a broad MMP inhibitor, GM6001 (Fig. S3A and B), while the inhibitor successfully suppressed MMP-dependent degradation of the gelatin matrix by invadopodia in MDA-MB-231 human breast cancer cells (Fig. S3C). Based on these observations, we inferred that this gelatin remodeling was due to mechanical detachment rather than enzymatic degradation.

Actomyosin-dependent contraction is required for SF-mediated ECM remodeling and invasion of SGC cells

Mechanical remodeling of the ECM requires cellular force generated by actomyosin-mediated contractility [6,20]. Immunofluorescence analysis revealed that signals for phospho- myosin light chain 2 (MLC2), an indicator of actomyosin contractility [21], were significantly stronger in CaF37 cells cocultured with 44As3 cells than in those cultured alone (Fig. 3A). Immunoblot analysis also showed that cocultured 44As3 and CaF37 cells have a higher level of MLC2 phosphorylation than in individually cultured cells or in a mixture of these cell lysates (Fig. 3B). Although αSMA and vimentin are strongly expressed in CaF37 cells, the expression levels were unchanged by co-culturing them with 44As3 cells (Fig. 3B). Treatment with a myosin II inhibitor blebbistatin nearly completely blocked disruption of the gelatin matrix and the formation of invasive foci by 44As3 and CaF37 cells (Fig. 3C–F). In contrast, GM6001 treatment did not affect these processes (Fig. S3D and E). These results indicate that actomyosin-mediated contractility is necessary for mechanical remodeling of the ECM during invasion by SGC and SFs.

Inhibitor library screening identified Rock and Src as critical regulators of the formation of invasive foci

To further gain the mechanistic insights into the formation of invasive foci, inhibitor screening was carried out with the SCADS

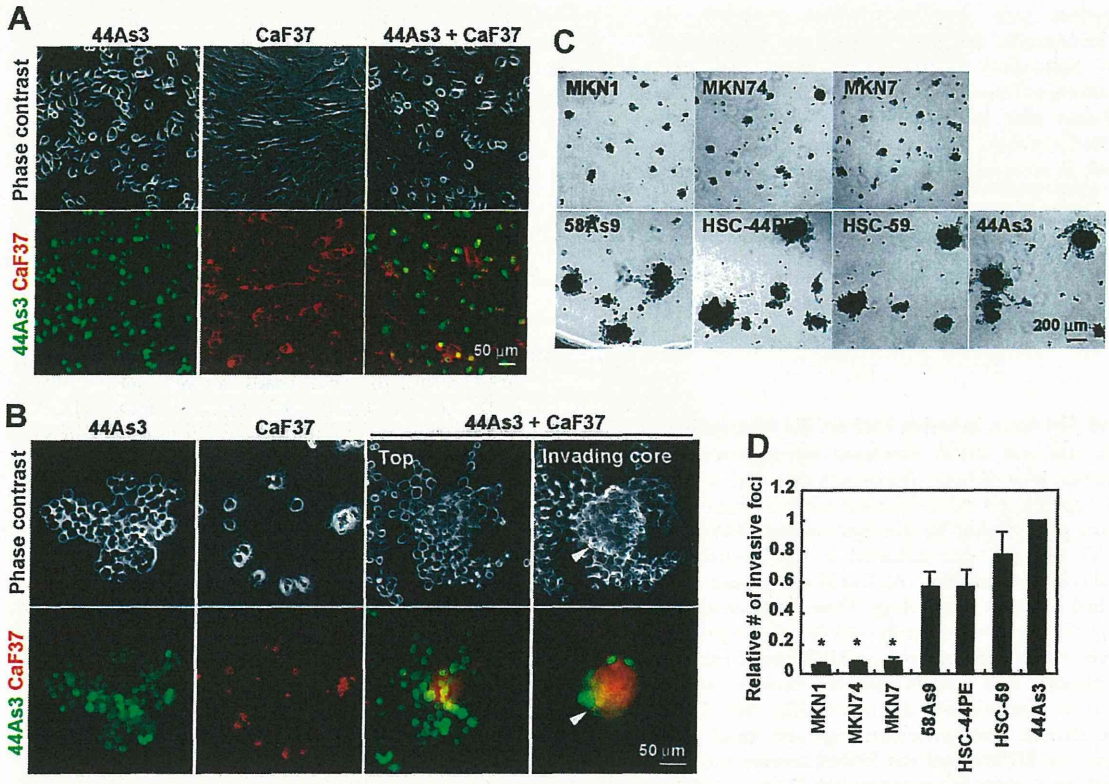

Figure 1. Formation of invasive foci by SGC cells and SFs on 3D Matrigel. A and B, 44As3 and CaF37 cells were labeled with CellTracker and cultured individually or together on either 2D (A) or 3D (B) Matrigel for 2 days. C, Non-SGC gastric cancer cell lines (MKN7, MKN1, and MKN74) and SGC cell lines (58As9, HSC59, HSC44PE, and 44As3) were cocultured with CaF37 cells on 3D Matrigel for 2 days. D, The relative number of invasive foci formed by CaF37 and indicated gastric cancer cell lines. Bars show mean ± SEM ($n=4$). *, $p<0.005$ vs SGC cell lines, by ANOVA with Tukey's test.
doi:10.1371/journal.pone.0085485.g001

inhibitor kit, which consists of 292 compounds, including well-known antitumor agents and molecular target drugs. As a result of quantitative analysis, several inhibitors that potently inhibited the formation of invasive foci were identified (Table S1 and Fig. S4). Cytotoxicity against individually cultured 44As3 and CaF37 cells was also determined to exclude compounds with non-specific effects (Table S1). We focused on H1152 and dasatinib, inhibitors for Rock and Src/Abl, respectively, for further analyses, because they have less cytotoxicity and exhibited strong inhibitory effects on the formation of invasive foci (Table S1), as confirmed by detailed fluorescent microscopic and quantitative analyses (Fig. 4A and B). In addition, cells treated with H1152 exhibited unique phenotypes (Fig. 4A): they formed flat and dispersed cell clusters that were interconnected with multicellular extensions. Although both inhibitors moderately suppressed cell growth of 44As3 and CaF37 cells at higher concentrations, they more efficiently blocked the formation of invasive foci (Fig. 4C): IC50 values were approximately 36 nM for dasatinib and 1.7 μM for H1152.

Rock regulates actomyosin contractility by directly phosphorylating MLC [22]. H1152 treatment significantly reduced phosphorylation of MLC2 in co-cultured 44As3 and CaF37 cells (Fig. 4D) and also strongly inhibited disruption gelatin matrix (Fig. 4E and F). Time-lapse observations revealed that although 44As3 and CaF37 cells still migrated and interacted each other by extending cellular protrusions even after treatment with H1152, following compaction of cell clusters was severely impaired as compared with control DMSO-treated cells (Video S5 and S6). This resulted in the formation of loosely packed flat cell clusters that were interconnected with cell protrusions and scarcely invaded into Matrigel.

44As3 and CaF37 cells treated with dasatinib remained single cells or small cell clusters on 3D Matrigel and did not efficiently form invasive foci (Fig. 4A and B). Time-lapse imaging demonstrated that cell migration and interaction were markedly inhibited by dasatinib treatment (Video S7). However, in contrast to H1152, dasatinib did not affect MLC phosphorylation (Fig. 4D) nor disruption of gelatin film in 2D coculture condition (Fig. 4E and F). These results indicate that dasatinib inhibits early stages of invasive foci formation, i. e. cell migration and cell-cell interaction, rather than actomyosin-mediated contraction and ECM remodeling. To test this hypothesis, we further characterized the effects of dasatinib. The ability of 44As3 and CaF37 cells to aggregate on 3D Matrigel was analyzed by calculating the areas and number of cell clusters in both individual and coculture conditions (Fig. 5A and B). Dasatinib treatment significantly reduced the areas of cell clusters and concomitantly increased the number of cell clusters in both cell types irrespective of the culture condition. Moreover, cell migration of both 44As3 and CaF37 cells on 3D Matrigel, as determined by calculation of the total and net migration distances from time-lapse movies, was suppressed by dasatinib treatment (Fig. 5C). Invasion depth of cocultured 44As3 and CaF37 cells within invasive foci as well as individually cultured CaF37 cells was also markedly reduced by dasatinib treatment (Fig. 5D). These results suggest that dasatinib impairs cell migration and interaction

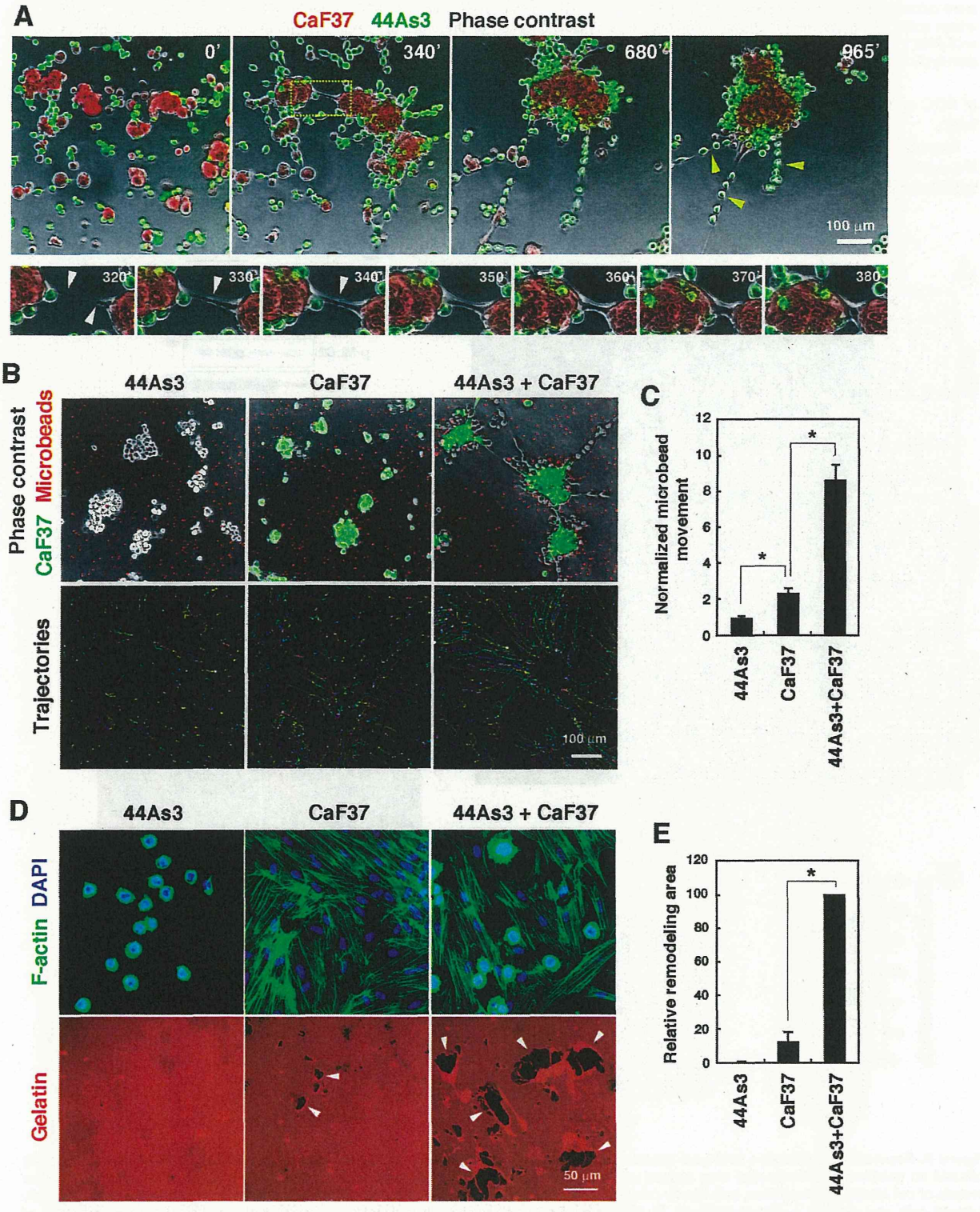

Figure 2. Imaging of the formation of invasive foci and concomitant remodeling of ECM. A, Time-lapse imaging of 44As3 and CaF37 cells cultured on 3D Matrigel. Yellow arrowheads denote chain-like structures formed by 44As3 cells. Lower panels are magnified image sequences of the boxed region. White arrowheads denote cell protrusions of CaF37 cells. B, Movement of the microbeads that were embedded in 3D Matrigel was tracked for 9 h and trajectories of each bead were shown as colored lines. C, Quantification of the movement of microbeads. Bars show mean ± SEM ($n = 48$ beads analyzed). *, $p < 0.0001$ by Student's t-test. Similar results were obtained in three independent experiments. D, 44As3 and CaF37 cells

were cultured on fluorescent gelatin-coated cover slips for 16 h and stained for F-actin and the nucleus (DAPI). Arrowheads denote the black areas where gelatin matrices were removed from cover slips. E, Quantification of the areas of gelatin detachment. Bars show mean ± SEM ($n=6$). *, $p<0.0001$ by Student's t-test.
doi:10.1371/journal.pone.0085485.g002

of SGC and SFs and, therefore, blocks SF-mediated invasion of SGCs.

Dasatinib inhibits Abl kinase activity as well as Src [23]. Nevertheless, we thought the effect of dasatinib is attributed to the inhibition of Src activity, because PP2, another Src inhibitor with different spectrum, also significantly inhibited the formation of invasive foci in our inhibitor library screening (Table S1 and Fig. S4). Consistent with this hypothesis, PP2 effectively blocked the formation of invasive foci as potently as dasatinib, while an Abl inhibitor imatinib exhibited no suppressive effect, rather tended to

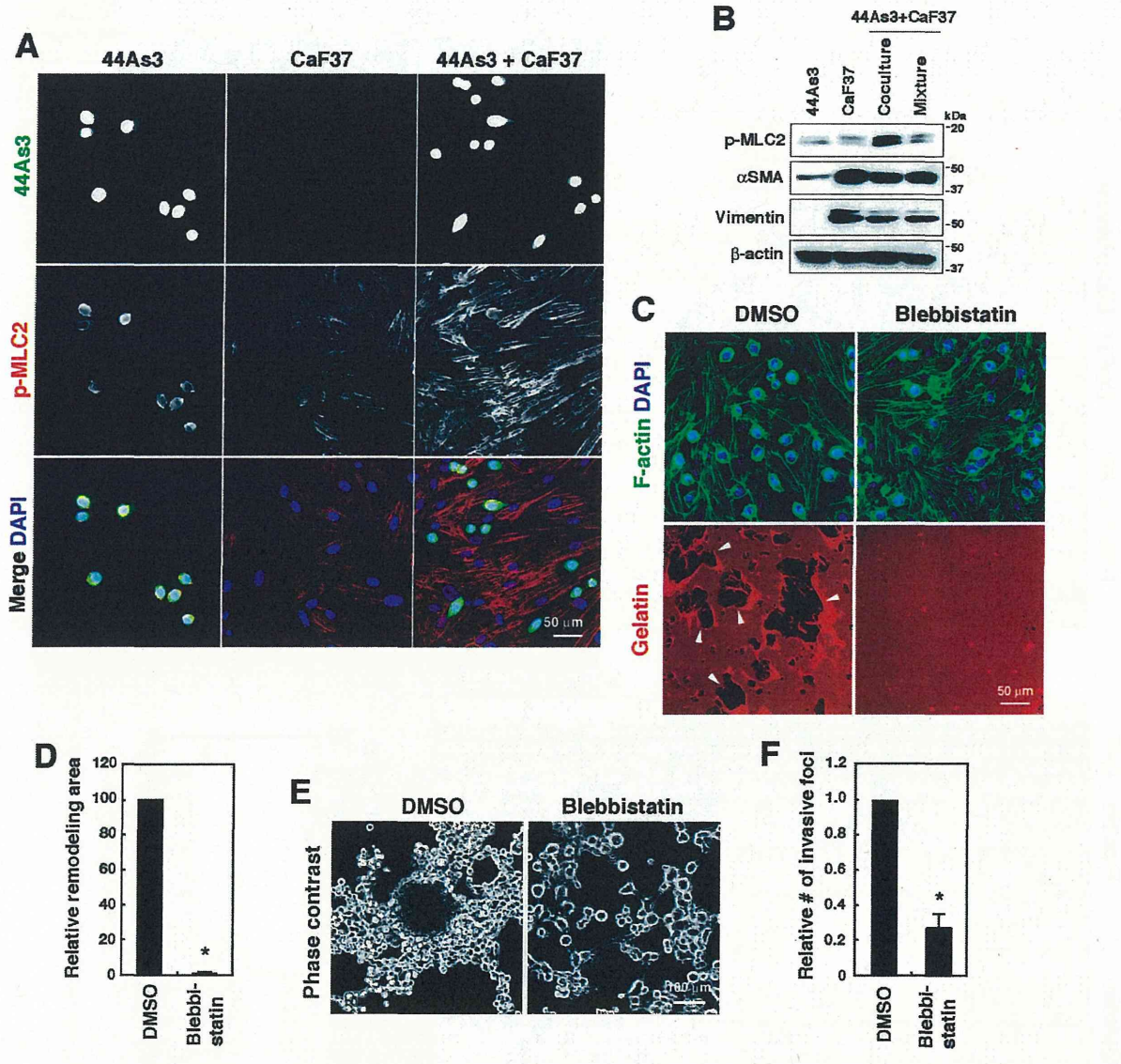

Figure 3. Formation of invasive foci and associated remodeling of ECM require actomyosin contraction. A, 44As3 and CaF37 cells cultured on gelatin-coated cover slips were stained with the antibody against phospho-myosin light chain 2 (p-MLC2) and DAPI. B, Immunoblot analysis of cell lysates prepared from individually cultured or cocultured (coculture) 44As3 and CaF37 cells. A mixture of cell lysates of individually cultured cells was used as a control (mixture). C, 44As3 and CaF37 cells were cultured on fluorescent gelatin in the absence or presence of blebbistatin (10 μM) for 16 h. Arrowheads denote the areas where gelatin matrices were disrupted. D, Quantification of the areas of gelatin disruption. Bars show mean ± SEM ($n=4$). *, $p<0.000001$ by Student's t-test. E, 44As3 and CaF37 cells were cocultured on 3D Matrigel in the absence or presence of blebbistatin (10 μM) for 2 days. F, The relative number of invasive foci was determined. Bars show mean ± SEM ($n=4$). *, $p<0.005$ by Student's t-test.
doi:10.1371/journal.pone.0085485.g003

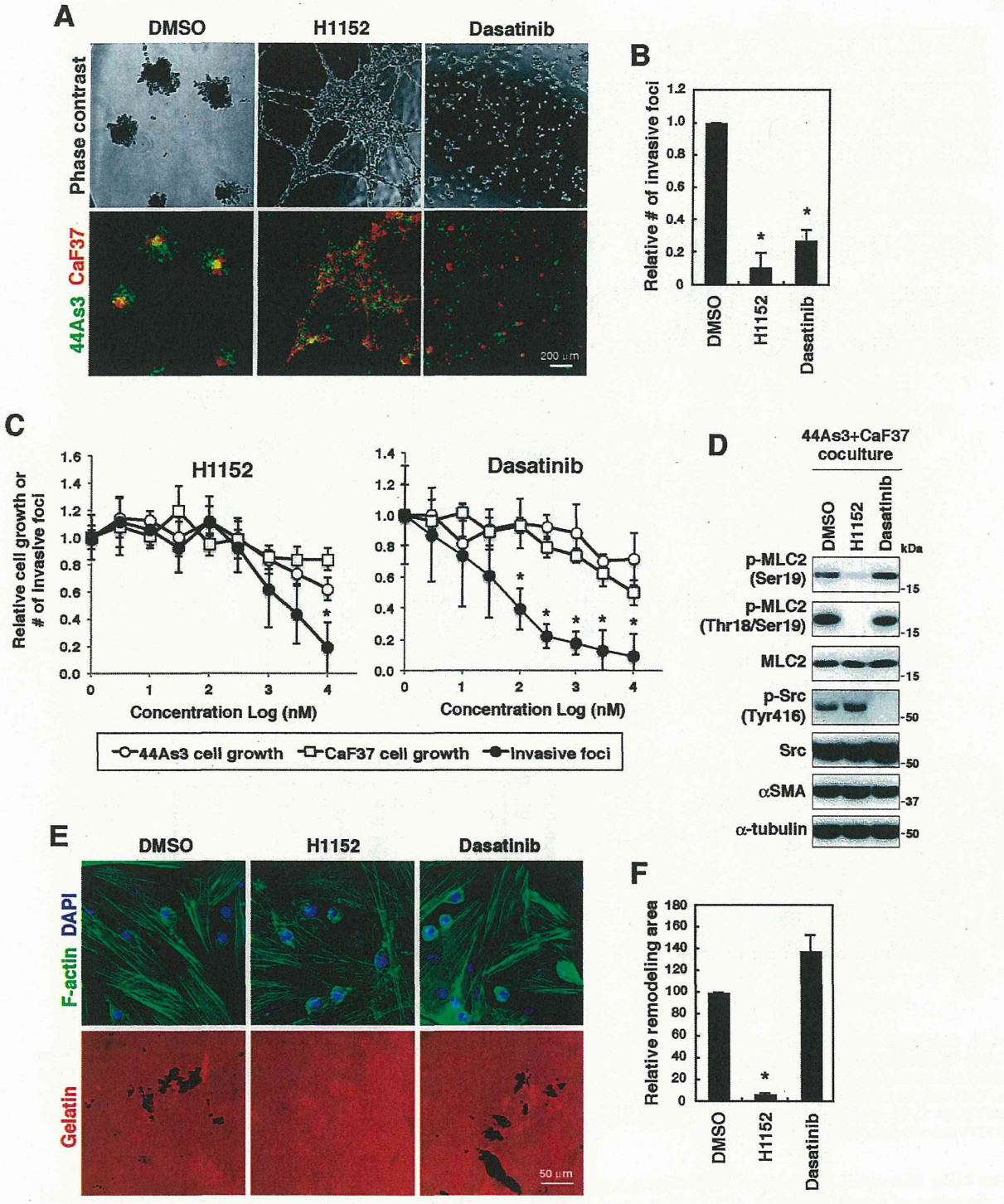

Figure 4. Rock and Src regulate the formation of invasive foci. A, 44As3 and CaF37 cells were plated onto 3D Matrigel in the presence or absence of H1152 (10 μM) or dasatinib (10 μM) for 2 days. B, Quantification of the number of invasive foci. Bars show mean ± SEM ($n=3$). *, $p<0.05$ by Student's *t*-test. C, Dose response effects of H1152 and dasatinib on cell growth of 44As3 and CaF37 cells and the formation of invasive foci. Bars show mean ± SD ($n=8$ for cell growth and 3 for invasive foci). *, $p<0.05$ by Student's *t*-test. D, Immunoblot analysis of 44As3 and CaF37 cells that were cocultured and treated with H1152 or dasatinib. E, The effect of H1152 and dasatinib on remodeling of the gelatin matrix. F, Quantification of the areas of gelatin disruption. Bars show mean ± SEM ($n=3$). *, $p<0.0005$ by Student's *t*-test.
doi:10.1371/journal.pone.0085485.g004

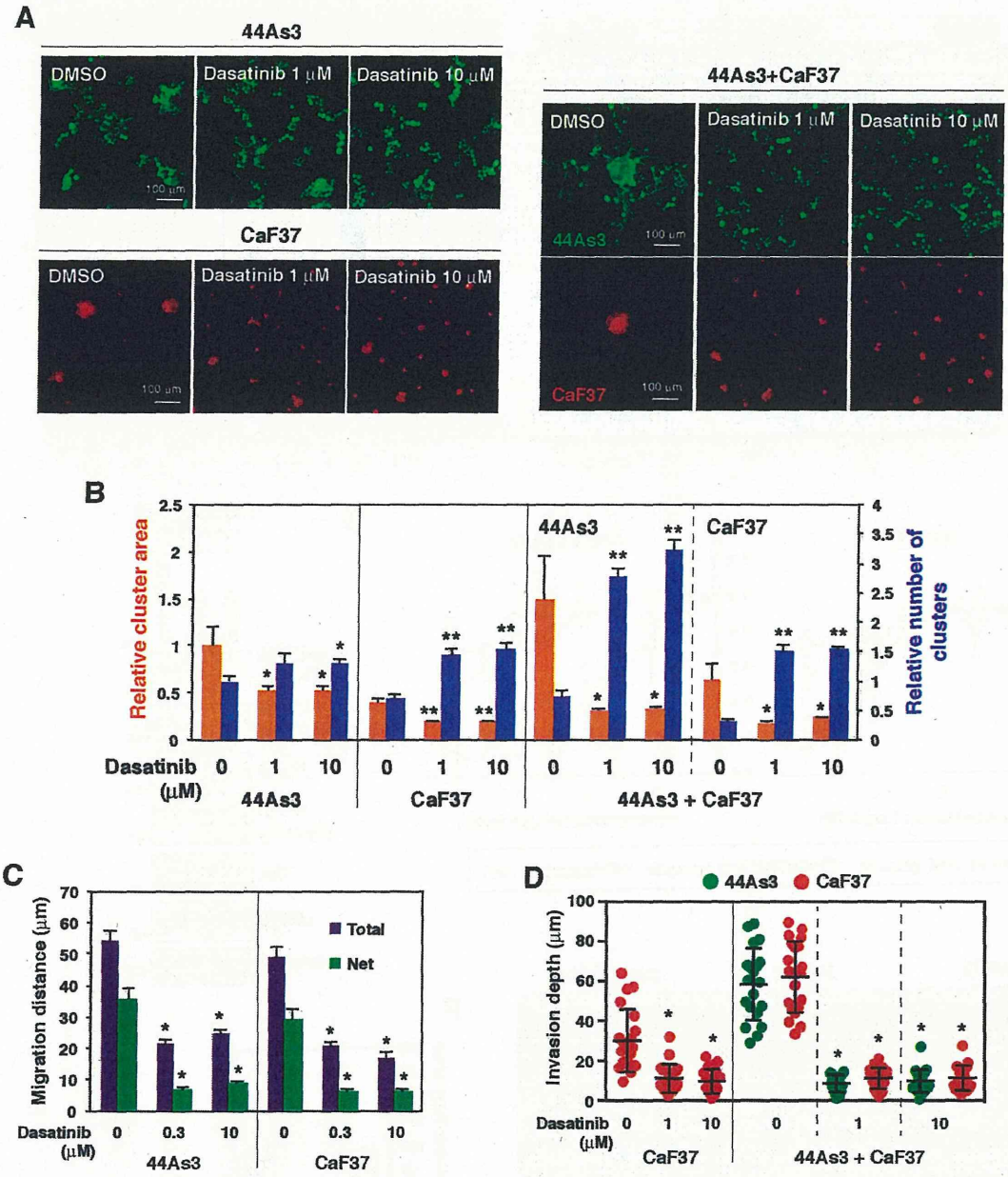

Figure 5. Dasatinib inhibits cell aggregation, migration, and invasion in vitro. A, Fluorescent images of individually cultured and cocultured 44As3 and CaF37 cells on 3D Matrigel in the presence or absence of dasatinib (1 or 10 μM) for 2 days. B, Quantification of the areas and number of cell clusters. Bars show mean ± SEM (n=48–502 for the cluster area, 6 for the number of clusters). *, $p<0.05$; **, $p<0.001$ by Student's t-test. C, Total and net migration distances of cells per hour were measured from time-lapse movies. Bars show mean ± SEM (n=40). *, $p<0.0001$ by Student's t-test. D, Invasion depth of the invasive foci or cell clusters. Bars show mean ± SD (n=20). *, $p<0.0001$ by Student's t-test.
doi:10.1371/journal.pone.0085485.g005

promote it (Fig. S5A and B). In addition, PP2 and imatinib did not affect disruption of gelatin by 44As3 and CaF37 cells in 2D coculture condition (Fig. S5C and D).

Finally, we investigated the effect of dasatinib on peritoneal dissemination of 44As3 cells in nude mice. Dasatinib treatment markedly reduced the number of tumor nodules formed on mesentery (Fig. 6A and B) and also suppressed ascites formation and dissemination to other tissues including omentum, parietal peritoneum, diaphragm, and liver (Table 1). We then performed immunofluorescence analysis of mesentery after injection of tdTomato-labeled 44As3 cells. This analysis revealed that SFs positive for a fibroblast marker FSP1 are accumulated at the boundary regions between tumor nodules and mesentery (Fig. 6C). Such accumulation of SFs was significantly impaired in mesentery treated with dasatinib. Histological analysis also revealed that the mesentery nodules from control mice were strongly associated with